Journal of Solid State Chemistry 279 (2019) 120954

Contents lists available at ScienceDirect

Journal of Solid State Chemistry

Structural, electronic and optical properties of $ABTe_2$ (A = Li, Na, K, Rb, Cs and B = Sc, Y, La): Insights from first-principles computations

L. Azzouz [a], M. Halit [a], M. Rérat [b], R. Khenata [c,*], Ajaya K. Singh [d], M.M. Obeid [e], Hamad R. Jappor [f,**], Xiaotian Wang [g,***]

[a] *Laboratoire Physique des Matériaux, Université Amar Telidji, BP.37G, Laghouat, 03000, Algeria*
[b] *IPREM UMR5254, CNRS / Université de Pau et des Pays de l'Adour, F-64000, Pau, France*
[c] *Laboratoire de Physique Quantique de la Matière et de Modélisation Mathématique (LPQ3M), Université de Mascara, 29000, Algeria*
[d] *Department of Chemistry, Government V.Y .T.PG Autonomous College Durg, Chhattisgarh, India*
[e] *Department of Ceramic, College of Materials Engineering, University of Babylon, 51002, Hilla, Iraq*
[f] *Department of Physics, College of Education for Pure Sciences, University of Babylon, Hilla, Iraq*
[g] *School of Physical Science and Technology, Southwest University, Chongqing, 400715, PR China*

ARTICLE INFO

Keywords:
Energy photoconversion
$ABTe_2$ (A = Li, Na, K, Rb, Cs and B = Sc, Y, La)
Atomic charges
Dielectric constant
Exciton binding energy
First-principles calculations

ABSTRACT

In this contribution, ternary telluride $ABTe_2$ compounds are proposed as promising candidates for *n*-type semiconductor materials in photovoltaic and photochemical devices. We report the successful calculations of the most fundamental properties needed in the previous applications such as the effective mass, dielectric constant and the exciton binding energy. This latter one has been evaluated from the density functional theory (DFT) method in the first time for these materials. An easy dissociation for hole-electron pair is suggested due to the small value of exciton binding energy at room temperature (i.e., lower than the thermal energy, 25 meV) for most of the studied compounds. The band structure and density of states of $ABTe_2$ are calculated using the hybridHSE06 functional, PBE0 and in addition the pure GGA-PBE functionals. Additionally, to elucidate the optical properties of these compounds, the complex dielectric function and optical reflectivity were computed for a wide range of photon radiation. Therefore, $ABTe_2$ materials are expected to be promising candidates for visible light driven photovoltaic and photocatalytic devices.

1. Introduction

Since the most abundant renewable energy resource is the solar energy, the study of photovoltaic and photochemical devices is the subject of many recent researches [1]. Light absorption, exciton dissociation and diffusion of charge carriers are the most important steps to convert the energy of light into other forms of energy such as electricity or chemical reaction [2]. The material must be able to absorb the light. In the case of photovoltaic or photochemical applications, the optimum band gap amid 1.4 and 3 eV (i.e. in the visible spectrum) is required [3–6]. The nature of the energy band gap (i.e. direct or indirect) has an evident effect on the type and nature of electronic transition [7,8]. The flat curve of the maximum bands (BV and BC) has also an important role in the case of sunlight absorption and for photovoltaic application since it modifies the absorption amount of the material [9].

The pair electron-hole (so-called exciton), that created during light absorption step, must be separated to giving free charge carriers that are used in the working of the device. This process is called "exciton dissociation". The binding energy of the exciton noted E_b is the electron-hole energy which must be as low as possible to facilitate the dissociation. Thermal energy is able to dissociate the exciton means that the E_b should be less than K_BT. The electrostatic force being proportional to the inverse of the static dielectric constant, a small value of the binding energy is provided with a large static dielectric constant. In Refs. [10–15], we can be noticed that the E_b values smaller than 25 meV that obtained for materials used in photovoltaic devices with a dielectric (ε_r) value larger than 10. For ionic systems the static, dielectric constant, including vibrational contribution in addition to the electronic one, is used in the

---

* Corresponding author.
** Corresponding author.
*** Corresponding author.
E-mail addresses: khenatat_rabah@yahoo.fr (R. Khenata), hrjms@yahoo.com (H.R. Jappor), xiaotianwang@swu.edu.cn (X. Wang).

https://doi.org/10.1016/j.jssc.2019.120954
Received 29 June 2019; Received in revised form 6 September 2019; Accepted 8 September 2019

estimation of the binding energy assuming that the time scale of the exciton dissociation is larger than the period of the harmonic modes [2].

Diffusion of charge carriers distinguishes by free charge carriers and move separately, which have been used in PV system electrodes or photochemical sites in a photocatalytic device. The mobility of the charge carriers and their related effective masses (m^*) are important parameters in the applications of light energy conversion, in which high mobility means low effective mass. Generally, the largest effective masses found in photovoltaic devices are less than 0.5 m_o allowing a good mobility [14,16–18].

In this work, an *ab initio* study on ternary $ABTe_2$ compounds (where A is Li, Na, K, Rb, Cs; and B is Sc, Y or La) is used in order to determine the following fundamental parameters such as: E_g, m^*, ε_r and E_b. The $ABTe_2$ compounds have rhombohedral (space group number 166), trigonal (space group number 164) and hexagonal (space group number 194) type-structures [19–21]. The $RbYTe_2$, $KYTe_2$ and $KLaTe_2$ compounds are synthesized by M. Babo et al. [20] and by K. Stöwe [19] respectively. On the other hand, the compounds $LiYTe_2$, $NaYTe_2$, $RbLaTe_2$, $CsScTe_2$ and $CsYTe_2$ are studied theoretically by J. Shi et al. [21]. The $ABTe_2$ structure depends on the ionic radius of rare earth R^{+3} and the fractional coordinate [19,21]. Homologous compounds of our studied materials i.e. ABS_2 have being intensively searched on their scintillation and luminescence properties, due to their potential applications for X-ray and white light-emitting diodes luminophores [22–27]. Most of these materials are wide band gap semiconductors >3 eV [22], and are not interesting in photovoltaic applications. From a chemical point of view, the electronegativity plays an important role in the band gap width: the electronegativity of the chalcogen atoms decreasing from S to Te (S = 2.58, Se = 2.55, Te = 2.10) leads to the decrease of the band gap of ABX_2 from X = S to Te [28–31]. That is why we predict a suitable gap for photovoltaic or photochemical applications with X = Te. Except the crystal structure and some electronic properties, most of the essential physical properties for $ABTe_2$ series are unknown. With this motivation, the theoretical detailed study of the structural, electronic and optical properties of the investigated $ABTe_2$ ternary telluride has been executed employing the first principles calculations.

2. Computational details

This work has been carried out using first-principal calculations under DFT field [32] as implemented in CRYSTAL code [33]. Three different Hamiltonians from GGA-PBE [34], PBE0 [35] and HSE06 [36,37] have been used to treat the exchange-correlation interactions. For all studied compounds here, the basis sets used in the present work are: the 61-1G (Dovesi et al. 1984) basis set [38] for Li, 8-511G (Dovesi et al. 1991) basis set [39] for Na, the HAYWSC-31 pseudo-potentials [40] for K, Rb and Cs, while Sc, Y, La, and Te are described by HAYWSC-311d31 (Bredow 2006) [41], ECP HAYWSC [40], 9761111sp-631d [40] and *m*-pVDZ-PP (Heyd et al. 2005) [42] basis sets, respectively. It is important to notice that the basis sets of Sc, Y, La and Te atoms have been modified in the present study. Reciprocal space is sampled using shrinking factor equal to 10, corresponding to 116 k-points in the irreducible Brillouin zone (IBZ) using Monkhorst-Pack k-points mesh [43] for all compounds.

For more precision, the threshold on the root-mean-square gradient and displacement was set to 10^{-4} a.u. The convergence criterion for the SCF cycle was fixed at 10^{-8} Hartree per unit cell during geometry optimization and dielectric constant calculations. The Broyden-Fletcher-Goldfarb-Shanno (BFGS) algorithm [44] which provides a fast way to find the minimum energy is used to determine the structural *a*- and *c*-parameters and the inter-atomic distances.

Frequency-dependent CPHF calculations of the dynamic dielectric properties in the range of photon energy have also been performed. In the coupled-perturbed (CP) method, orbitals relaxation was taken into account in the presence of the external field (see details in Ref. [45]).

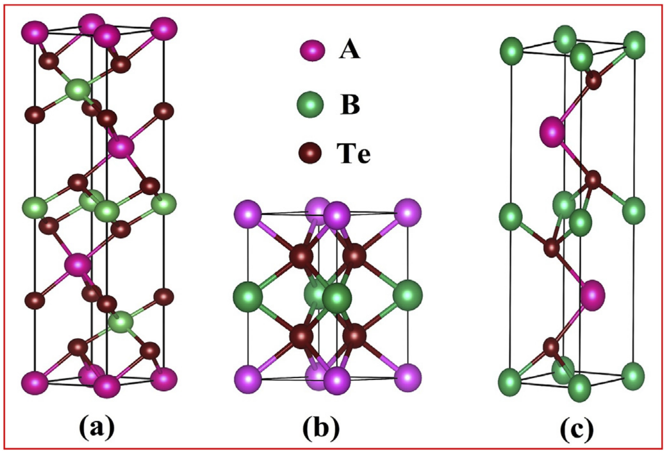

Fig. 1. Crystal structure of $ABTe_2$ compounds (**a**: rhombohedral with $R\overline{3}m$; **b**: trigonal with *P-3m1*; **c**: hexagonal structure with $P6_3/mmc$ space group).

3. Results and discussions

3.1. Structural properties

The studied $ABTe_2$ (where A is Li, Na, K, Rb, Cs; and B is Sc, Y or La) materials crystallized in three type structures: trigonal, rhombohedral and hexagonal. Firstly, the $LiYTe_2$ compound crystallizes in the trigonal-I type structure with the *P-3m1* space group and with two formula units per unit-cell (Z = 2). $NaYTe_2$, $KYTe_2$, $KLaTe_2$, $RbLaTe_2$, $CsScTe_2$ and $CsYTe_2$ compounds crystallize in the $R\overline{3}m$ trigonal-II type structure and three formula units per unit-cell (Z = 3), while $RbYTe_2$ compound crystallizes in the *P63/mmc* hexagonal-type structure and two formula units per unit-cell (Z = 2). The trigonal-type structure can be described as a distorted pseudo-cubic along the [111] direction packed of Telluride atoms with the stacking ABCA sequence and with the ABBA sequence for the hexagonal-type structure (i.e. in $RbYTe_2$). Both cations (A^{+1} and B^{+3}) are situated in alternating layers with octahedral and trigonal prismatic interstices according to the trigonal and hexagonal structures. Projections of the $ABTe_2$ structures (trigonal and hexagonal) are presented in Fig. 1. The good reproduction of the cell parameters is essential for the semiconductor study, since a bad agreement between theory and experiment will induce a poor description of electronic properties. The structural parameters: *a*, *c*, and bond-length, are collected in Table 1 for comparison with the other available results in the literature. We can observe that there is a fairly good agreement between DFT and experiment (Refs. [19–21]).

From the functionals point of view, the best results are found at the PBE0 level with a relative error of 2 and 9% on *a*- and *c*-parameters compared to the experimental and other theoretical values, (see Table 1). We can see that the lattice parameters increase from $LiYTe_2$ to $CsYTe_2$ with the alkaline radius size (see Fig. 1). This trend is also noticed for bond-lengths. Similar results were also found in different previous studies for cell-parameters: $a_{(NaLaSe2)} = 4.34$ Å, $a_{(KLaSe2)} = 4.40$ Å, $a_{(RbaLaSe2)} = 4.43$ Å; $c_{(NaLaSe2)} = 20.79$ Å, $c_{(KaLaSe2)} = 22.78$ Å, $c_{(RbaLaSe2)} = 23.71$ Å in Refs. [46–48], and for bond-length, $d_{K\text{-}Te} = 3.24 < d_{Rb\text{-}Te} = 3.64$ Å in Ref. [20].

3.2. Band gap

As mentioned in the introduction, semiconductors must have an optimum band gap larger than 1.4 and less than 3.0 eV to be possible candidates for photovoltaïc and photochemistry [49,50]. On the other hand, the amplitude of the dipole moment interband transitions from $i(k) \rightarrow j(k')$ defining their band gap or visible absorption energy determines the intensity of the light energy conversion processes.

Table 1
The calculated structural parameters and bond length of $ABTe_2$: lattice parameters (a, c, d, in Å).

	Parameters	$LiYTe_2$	$NaYTe_2$	$KYTe_2$	$KLaTe_2$	$RbYTe_2$	$RbLaTe_2$	$CsScTe_2$	$CsYTe_2$
PBE	a	4.25	4.40	4.49	4.47	4.53	4.79	4.43	4.59
	c	7.15	22.63	24.74	24.90	17.22	26.08	26.89	27.11
	$d_{(A\text{-}Te)}$	3.00	3.24	3.40	3.71	3.67	3.76	3.84	3.85
	$d_{(B-Te)}$	3.07	3.08	3.22	3.25	3.12	3.29	3.02	3.15
PBE0	a	4.24	4.39	4.47	4.73	4.51	4.77	4.40	4.56
	c	7.12	22.50	24.67	24.81	17.19	25.97	26.86	27.07
	$d_{(A\text{-}Te)}$	2.99	3.23	3.53	3.58	3.68	3.74	3.86	3.87
	$d_{(B-Te)}$	3.06	3.08	3.09	3.27	3.10	3.28	2.98	3.12
HSE06	a	4.25	4.39	4.48	4.73	4.51	4.78	4.40	4.57
	c	7.14	22.55	24.68	24.83	17.19	25.99	26.86	27.08
	$d_{(A\text{-}Te)}$	3.00	3.23	3.53	3.59	3.68	3.75	3.86	3.88
	$d_{(B-Te)}$	3.06	3.08	3.09	3.27	3.10	3.28	2.98	3.12
Others	a	4.30[a]	4.43[a]	4.39[b]	4.66[c]	4.43[b]	4.74[a]	4.37[a]	4.55[a]
	c	7.15[a]	22.70[a]	22.55[b]	24.41[c]	17.29[b]	25.60[a]	26.50[a]	26.74[a]
	$d_{(A\text{-}Te)}$	3.03[a]	3.26[a]	3.24[b]	3.53[c]	3.64[b]	3.71[a]	3.78[a]	3.81[a]
	$d_{(B-Te)}$	3.09[a]	3.10[a]	3.07[b]	3.23[c]	3.08[b]	3.25[a]	2.98[a]	3.12[a]

[a] Ref. [19].
[b] Ref. [18].
[c] Ref. [17].

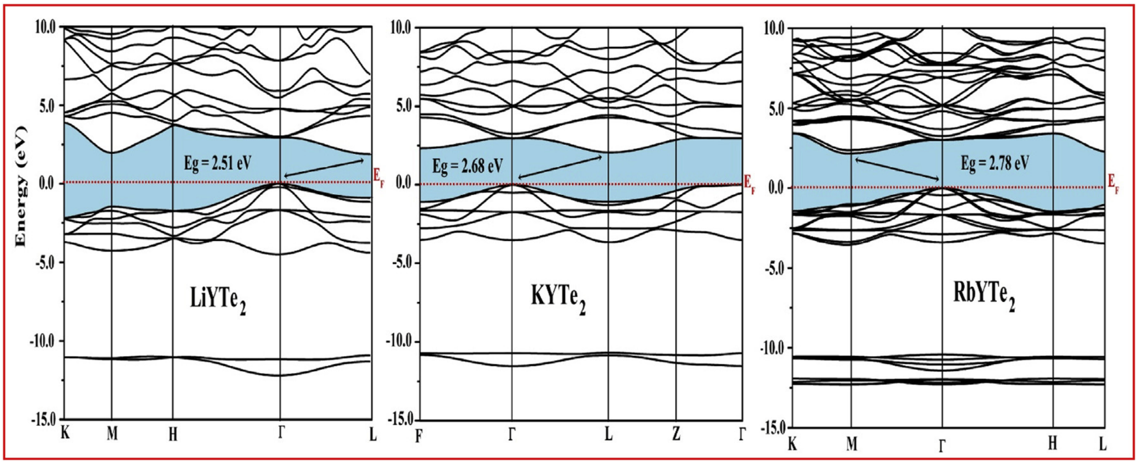

Fig. 2. The calculated band structure spectra along the high-symmetry lines for $LiYTe_2$, $KYTe_2$ and $RbYTe_2$ by PBE0. The Fermi level is set to zero energy.

Calculations of the electronic energy band structure have been performed by PBE, PBE0 and HSE06 functionals on a discrete grid of points along lines connecting high symmetry k-points in Brillouin zone (BZ). Because we have three different phases, we show in Fig. 2 the $LiYTe_2$, $KYTe_2$ and $RbYTe_2$ band diagrams as representative for the trigonal-I, –II and hexagonal phases, respectively. The Fermi energy level is located at the maximum band valence. As well be seen in Fig. 2, the highest occupied valence band is located in **Γ** and the lowest unoccupied one in the conduction band is located in **L** and **M** points for $LiYTe_2$, $KYTe_2$ and $RbYTe_2$, respectively, which indicates that these materials are characterized by an indirect band gap. Even more interesting is that the band gap is direct for the entire material system. This is in contrast to the understudy $ABTe_2$ materials whose band gap is indirect for high band gap alloys. The calculated direct and indirect band gap values for the investigated structures at the level of different exchange-correlation tabulated in Table 2, which also contains results of the previous calculations. It is well known that pure DFT Hamiltonian as LDA and PBE underestimates band gap values with respect to experimental ones, while Hartree-Fock (HF) provides too large values. The present results of band gap with the hybrid HSE06, PBE0 Hamiltonians show an enlarging by comparison with PBE-GGA for all compounds. HSE06 showed a good agreement with available theoretical results and less about 0.7 eV compared to those calculated by PBE0. As a consequently, we predict a shifting of optical spectra to high energy (i.e. about 0.7 eV/200 nm to UV) for PBE0. We observe from Table 2 that the increasing of alkali ionic radii from Li to Cs increases the band gap width (1.88 for $LiYTe_2$ to 2.28 eV for $CsYTe_2$). This suggests that the absorption quantity to sunlight for the $LiYTe_2$ and $NaYTe_2$ materials will be higher than the other compounds (see in

Table 2
The calculated energy band gap of $ABTe_2$ (in eV), direct values in parentheses.

	$LiYTe_2$	$NaYTe_2$	$KYTe_2$	$KLaTe_2$	$RbYTe_2$	$RbLaTe_2$	$CsScTe_2$	$CsYTe_2$
PBE	1.20(2.14)	1.13(2.07)	1.36(2.13)	1.51(2.35)	1.47(2.18)	1.61(2.36)	1.19(1.51)	1.58(2.19)
PBE0	2.51(3.58)	2.38(3.51)	2.68(3.61)	2.80(3.78)	2.78(3.66)	2.92(3.80)	2.59(3.05)	2.28(3.02)
HSE06	1.88(2.94)	1.78(2.87)	2.58(2.95)	2.18(3.12)	2.16(3.01)	2.29(3.14)	2.13(2.97)	2.28(3.02)
Others	1.56(2.48)[a]	–	–	–	2.30(2.87)[a]	1.64(2.20)[a]	2.03(2.76)[a]	1.56(2.48)[a]

[a] Ref. [19].

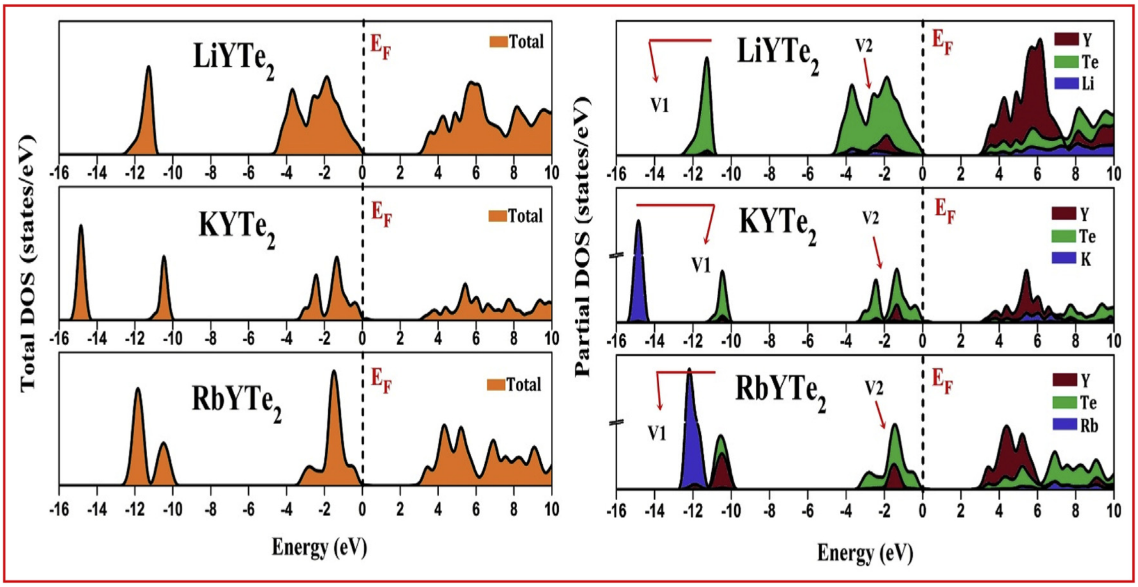

Fig. 3. The calculated DOS diagrams for $LiYTe_2$, $KYTe_2$ and $RbYTe_2$ by PBE0. The Fermi level is set to zero energy.

spectrum of Imagine part of Epsilon). Moreover, the maximum *E(k)* dispersion is observed in the **Γ-Γ** direction near the Fermi region, whereas there is a quasi-flat band in the **Γ-Z** (or **Γ-L**) direction. As a direct result, we expect lesser effective masses for the charge carriers and high mobility, enhancing charge-carrier kinetic for these materials. To further explain and elaborate the nature of the electronic states of the energy bands, we have calculated the total partial densities of states (DOS) diagrams. Fig. 3 reports DOS of $LiYTe_2$, $KYTe_2$ and $RbYTe_2$. It can be seen that the valence band (VB) is formed by two regions: **V1** and **V2** (see Fig. 3), the first region (**V1**) around −15 and −11 eV mainly *p*-A, *s*-Te and a little *p*-B states contribution are located. Interestingly, *p*-A states shift to slightly lower energy values going from 15 and -12 eV. The second region (**V2**) around −3.7 eV is dominated by *p*-Te states hybridized with a small contribution of *d*-B states. In the conduction band (CB), *d*-B states as well as *s* and *p* states are the main components with a minor contribution from *p*-Telluride states. Then, the optical gap is mainly determined by the main transition between Te^{-2} valence bands to B^{+3} conduction bands. Material with a band gap between 1.4 and 3 eV, can be used in visible light energy conversion [3,50,51]. Thus, all considered materials have a gap less than 3 eV (see Table 2), which means that they can be used in visible light energy applications.

In the next step, we will discuss the most fundamental properties (effective mass m^*, dielectric constant ε_r, and exciton binding energy E_b required from a semiconductor to make it useable in photovoltaic and photochemical devices.

3.3. Effective mass

The effective mass can be found by fitting the *E*-*k* diagram around the conduction band minimum (CBM) for the electrons or the valence band maximum (for the holes) by a parabola, which takes into account the electrons behavior almost like free electrons in the extremity bands (i.e. BV and BC extremum). Thus, the effective mass is then obtained from,

$$\frac{1}{m^*} = \frac{1}{\hbar^2}\frac{\partial^2 E(K)}{\partial^2 K}. \tag{1}$$

Electrons with energy close to the valence band maximum behave almost like free electrons. Thus, their effective mass plays a role in the potentially high mobility of charge carriers and also in the binding energy of the exciton (see below). The computed effective masses of the investigated materials are reported in Table 3 in which the effective electron mass is point out by under script “*e*’’ (m_e^*) and the hole mass by

Table 3
The computed effective masses (m^*) (in electron mass), dielectric constants (ε_r) and binding energy (E_b) (in meV).

	Parameters	$LiYTe_2$	$NaYTe_2$	$KYTe_2$	$KLaTe_2$	$RbYTe_2$	$RbLaTe_2$	$CsScTe_2$	$CsYTe_2$
PBE	m_e^*	0.94	0.31	0.42	0.34	0.29	0.36	1.23	0.62
	m_h^*	0.53	0.75	0.68	0.71	0.32	0.73	0.85	0.78
	ε_{vib}	10.73	9.89	8.08	9.90	7.90	9.92	9.13	7.78
	ε_∞	8.33	7.85	6.91	6.50	6.31	6.09	7.38	5.96
	$\varepsilon_0(\varepsilon_r)$	19.06	17.47	14.99	16.40	14.21	16.01	16.51	13.74
	E_b	12.68	9.77	15.71	12.20	10.25	12.79	25.08	24.88
PBE0	m_e^*	0.86	0.27	0.37	0.27	0.23	0.33	0.95	0.56
	m_h^*	0.62	0.73	0.62	0.60	0.31	0.77	0.84	0.79
	ε_{vib}	7.85	7.07	5.98	7.00	5.33	7.19	6.08	5.02
	ε_∞	6.73	6.47	5.86	5.38	5.29	5.16	5.82	5.04
	$\varepsilon_0(\varepsilon_r)$	14.58	13.53	11.84	12.38	10.62	12.35	11.90	10.06
	E_b	23.07	14.64	22.48	16.52	15.92	20.60	42.81	44.03
HSE06	m_e^*	0.89	0.29	0.38	0.28	0.25	0.33	0.96	0.58
	m_h^*	0.55	0.76	0.79	0.68	0.31	0.80	0.73	0.90
Others	m_h^*	0.61[a]	0.84[a]	–	–	–	1.10[a]	0.77[a]	0.80[a]

[a] Ref. [19].

“h'' (m_h^*). Generally, the different functionals give almost similar results. Here, the discussion will focus only on the effective mass calculation for these materials. Shi et al. [21] have been reported hole effective masses for $LiYTe_2$ (0.61m_o), $NaYTe_2$ (0.84 m_o), $RbLaTe_2$ (1.10 m_o), $CsScTe_2$ (0.77 m_o) and $CsYTe_2$ (0.80 m_o) calculated by HSE06. They are close to ours, (0.55 m_o, 0.76 m_o, 0.80 m_o, 0.73 m_o and 0.90 m_o for $LiYTe_2$, $NaYTe_2$, $RbLaTe_2$, $CsScTe_2$ and $CsYTe_2$, respectively) showing the accuracy of our calculation. In other side, the electron effective masses are smaller compared than hole masses for all studied compounds, except $LiYTe_2$ and $CsScTe_2$, which leads us to classify these semiconductors as *n*-type semiconductors materials. We noticed from literature that the effective mass for famous materials used in convert light energy devices have values less than 0.5 m_o and therefore, leading to a high mobility of charges [2]. This is the case for all the studied compounds except $CsScTe_2$. However, for $CsScTe_2$, its effective masses around the unity suggesting its mobility of carriers smaller compared to other compounds.

3.4. Dielectric constants

The polarization response of a dielectric material to the external incident electric field or radiation is presented by ε_r. Its static constant (ε_0) constitutes by two contributions in which the electronic part (noted ε_∞) presents the polarizability of the electron density and the vibrational one (noted ε_{vib}) reflects ions displacement in the crystal lattice. Hence, we have,

$$\varepsilon_0 = \varepsilon_\infty + \varepsilon_{vib} \tag{2}$$

The electronic contribution to the static dielectric tensor is calculated from an iterative coupled-perturbed Hartree-Fock/Kohn-Sham (CPHF/KS) process [52], with a threshold of 10^{-4} bohr^3 on the unit cell polarizability, while the vibrational contribution part is computed from the harmonic phonon spectrum using the equation,

$$\varepsilon_{vib} = \frac{4\pi}{V}\sum_p \frac{z_p^2}{\vartheta_p^2} \tag{3}$$

where V is the volume of the unit cell, ϑ_p and Z_p are the phonon frequency of the mode p and the Born effective charge respectively.

Moreover, the electronic dielectric ε_∞ part and the vibrational one ε_{vib} present the two contributions to the dielectric constant ε_0 in material. Table 3 shows results obtained from the coupled-perturbed PBE and PBE0 calculations. We notice that most values calculated by PBE0 are between 10 and 14, and the highest values are obtained for $LiYTe_2$ (14.58), $NaYTe_2$(13.53) and $KLaTe_2$ (12.38) compounds, make these materials have a smallest electron-hole electrostatic forces, and by consequence a smallest exciton energies binding. $CsYTe_2$ has a lower static dielectric value (10.06) which compromises its efficiency even if the band gap is in the favorable range as discussed above, and suggests that this compound has a largest exciton energy binding (discussed below). Both the obtained electronic and vibrational contributions to the static dielectric constant are larger with PBE than with PBE0 due to the too small gap value and too soft phonons.

3.5. Exciton binding energy

The exciton binding energy (E_b) can be evaluated using the Wannier exciton model [53] in which the exciton treats as a hydrogen atom. In this model, the calculation of E_b involves only the knowledge of the dielectric constant of the semiconductor and the effective masses of the charge carriers and it can be computed as follow,

$$E_b = E_H\frac{\mu}{\varepsilon_r^2} \tag{4}$$

where E_H is the energy of the 1s orbital of hydrogen (−13.6 eV), ε_r is the dielectric constant and μ is the reduced mass of exciton,

$$\frac{1}{\mu} = \frac{1}{m_e^*} + \frac{1}{m_h^*} \tag{5}$$

The binding energy must be smaller than the thermal energy (25 meV), to achieve an efficient dissociation of the exciton at room temperature, Because the time scale of the exciton dissociation in optoelectronic devices is higher than the atomic motions, it is assumed that the resulted charges (i.e. electrons and holes obtained from exciton dissociation) are governed by the relaxed exciton, then the relative dielectric constant in the binding energy expression (eq. (4)) is given by the static dielectric ε_0 constant (i.e. $\varepsilon_r = \varepsilon_0$) [2]. The obtained relaxed exciton binding energies are computed using ε_r values presented in Table 3. The exciton binding energies calculated by PBE are smaller than the PBE0 ones due to the overestimation of ε_r given by PBE as said previously. We can see from the literature, that there is a relation between the exact HF-exchange and $\frac{1}{\varepsilon_\infty}$ (the inverse of the electronic dielectric constant), in which the band gap is well reproduced. For this, we observe that the PBE0 (with 25% of HF exchange) is more reliable approximation for compounds having ε_∞ around 4 [54,55]. The exciton binding energy is larger than 25 meV for $CsScTe_2$ (42.81) and $CsYTe_2$ (44.03), which means that their exciton (electron-hole force) is strongly bounded and cannot be dissociated at room temperature. The smallest effective mass is obtained for $NaYTe_2$ (14.64), $RbYTe_2$ (15.92) and $KLaTe_2$ (16.52), see Table 3, so the easier diffusion of charge carrier is attributed to them. Moreover, their exciton binding energy is lower than the thermal energy (25 *meV*) compared to other $CsScTe_2$ and $CsYTe_2$.

Therefore, the efficiencies of $NaYTe_2$, $RbYTe_2$ and $KLaTe_2$ in light energy conversion will be wider. In the best of our knowledge, this is the first study was performed to determine these parameters in considered $ABTe_2$ compounds, and we welcome experiments to prove them.

3.6. Optical properties

The optical properties of a compound are very important to understand the nature of materials and also give a clear picture of their applications in photovoltaic or photochemical devices. Therefore, their dynamic optical properties like frequency dependent dielectric functions $\varepsilon(\omega)$ and reflectivity $R(\omega)$ are investigated in details in the 0–20 eV range of radiation energy by PBE0 functional with CP method for their possible applications in optoelectronics. The successfully calculated imaginary $\varepsilon_2(\omega)$ and real $\varepsilon_1(\omega)$ parts as functions of an electromagnetic wave-frequency allow us to calculate all other important linear optical characteristics.

As well known, the real part of dielectric function describes polarization and the imaginary one treats absorption. The latter one (imaginary part) is derived by the optical transitions between occupied and unoccupied bands [56]. In CRYSTAL, both parts of dielectric function are calculated in the same time at the self-consistent coupled-perturbed level of calculation. Fig. 4 shows the calculated CP-PBE0 results for the real part of the complex dielectric function, $\varepsilon_1(\omega)$. It is clear from the plots that the optical dielectric constant before resonances $\varepsilon_1(\omega = 0)$ increases with the decrease of the band gap energy for both directions of polarization, explaining why $CsScTe_2$ and $CsYTe_2$ have the smallest dielectric constant. Moreover, the plots reveal that the variation of the optical dielectric constant values for (001) direction is less remarkable than the component of (100) one. This mean that the understudy $ABTe_2$ materials have two dominant independent components of the dielectric tensor. The corresponding dielectric functions are $\varepsilon^X(\omega)$ and $\varepsilon^Z(\omega)$ corresponding to the applied electric field (light polarization) parallel and perpendicular to the crystallographic *c*-axis. At certain energy limit over resonances, $\varepsilon_1(\omega)$ drops below unity and the compounds show a metallic behavior.

Fig. 5 displays the energy position and relative amplitudes of specific absorption from the imaginary $\varepsilon_2(\omega)$ part of the dielectric response of $ABTe_2$ calculated by the CP-PBE0 method. The interband electronic transitions of the dielectric function can be split into direct and indirect transitions. We pay no attention to the indirect interband electronic

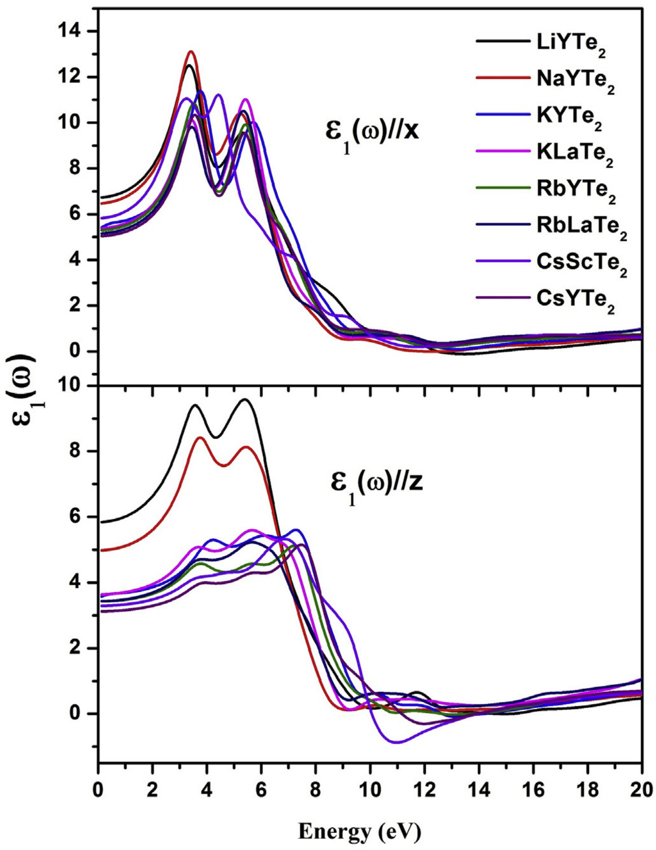

Fig. 4. The real part $\varepsilon_1(\omega)$ of the dielectric function of $ABTe_2$ compounds versus photon energy for different polarizations of the incident radiations at CP-PBE0 level of calculations.

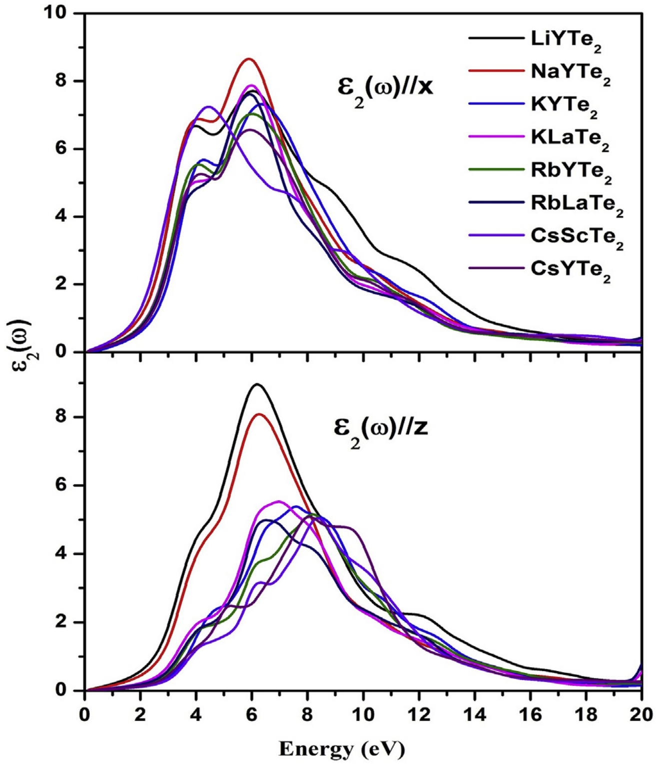

Fig. 5. The imaginary part $\varepsilon_2(\omega)$ of the dielectric function of $ABTe_2$ compounds versus photon energy for different polarizations of the incident radiations at CP-PBE0 level of calculations.

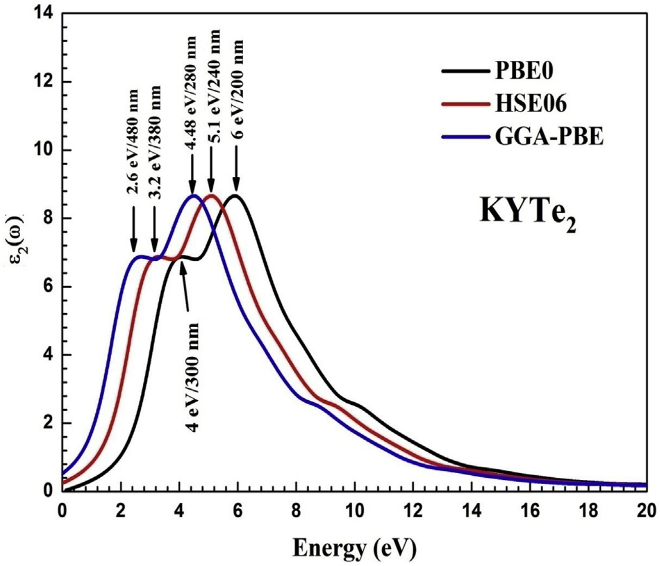

Fig. 6. Scissor correction effect on the $\varepsilon_2(\omega)$ spectra of $KYTe_2$ compound versus photon energy at CP-PBE0, HSE06 and GGA-PBE levels of calculations.

transitions that involving the scattering of phonons that are expected to produce a slight contribution to $\varepsilon(\omega)$. It is worthy to identify the origin of the direct interband $i(k) \rightarrow i'(k)$ electronic transitions between the occupied states in the VB and the unoccupied ones in the CB that are responsible for the main peaks of the $\varepsilon_2(\omega)$ spectra of the studied compounds with the help of their band gap diagrams. Our analysis of the $\varepsilon_2(\omega)$ spectra show two main peaks (optical critical points of the dielectric function) occur at 4 and 6 eV for all compounds, which are due to optical transitions from valence bands to conduction bands. These points are $\mathbf{\Gamma_V}$–$\mathbf{\Gamma_C}$, which give the threshold for the direct transitions between the valence and the conduction bands for the investigated compounds. Our outcomes are compared with the computed DOS and band structure to locate the source of these characteristics in the Brillouin zone. Hence, Fig. 6 shows the two critical points in linear optical transitions for $KYTe_2$. Indeed, the first critical point (4 eV) is mainly due to transitions between *d*-Y + *p*-Te valence bands to *s*/*d*-Y + *s*-Te conduction bands. The second critical point (6 eV) is due to *d*-Y + *p*-Te valence bands to *p*-K + *p*-Y + *s*-Te conduction bands. In light energy conversion, the absorption via $\varepsilon_2(\omega)$ should be in the visible spectrum. We note here, that the band gaps are overestimate by PBE0 and the CP-PBE0 spectra are shifted by around 0.8 eV/100 nm and around 1.4 eV/200 nm to UV region compared to HSE06 and GGA-PBE respectively. For correct the absorption spectra we used the scissor operator correction [57], their values were considered as 0.8 and 1.4 eV for HSE06 and GGA-PBE respectively see Fig. 6. $LiYTe_2$ and $NaYTe_2$ have smallest band gap values (Table 2), as consequently they show again their largest absorption in the visible spectrum predicting a better efficiency in photovoltaic applications.

The CP-PBE0 reflectivity spectrum $R(\omega)$ is shown in Fig. 7 for $ABTe_2$. The reflectivity does not approach the unity when the photon frequency tends towards zero, meaning that these materials behave like semiconductors and the $ABTe_2$ materials are transmitting for frequencies less than 2eV. Also, it is obvious from the Figure that the reflectivity increases with the increasing of incident photon energy (above 2.5eV). The computed $R(\omega)$ rises from interband transitions approximately by about 35% compared to its static R(0) reflectivity along 100 and 001 directions at about 3.5 and 6 eV, respectively. Moreover, the $R(\omega)$ is decreasing until 5% at energy larger than 17 eV for the series of materials. In the

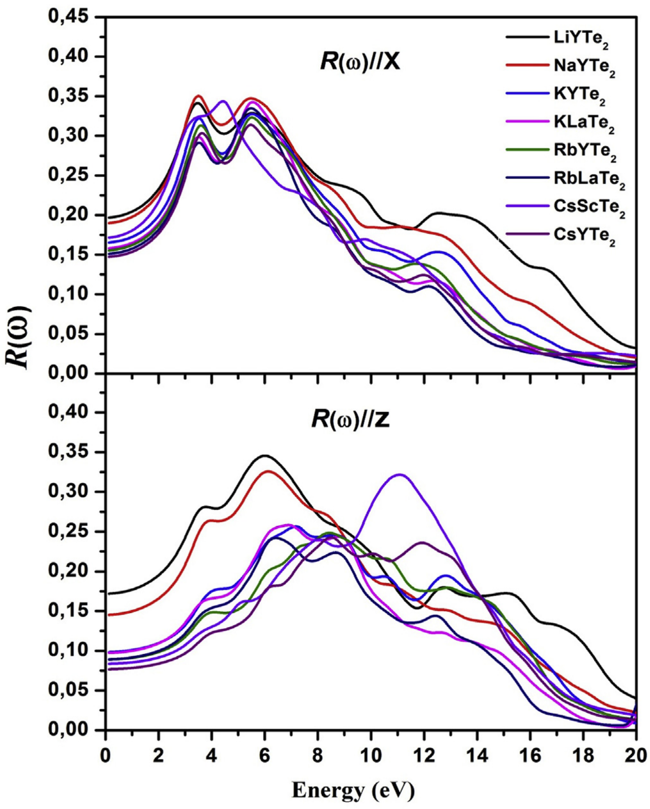

Fig. 7. The reflectivity $R(\omega)$ spectra of ABTe$_2$ compounds versus photon energy at CP-PBE0 level of calculations.

scientific literature R values for materials commonly used in the light conversion process are about or less than 40% in the visible energy range [58,59]. In Si, InP and GaP nanowire materials used for photovoltaic applications, we found their reflectivity values are between 30% −40% [60]. In addition, to ensure low reflectance amount in materials and by consequence high photon to electron conversion efficiencies, researchers made antireflection films to increase the absorption ratio [61–63].

4. Conclusions

In summary, the ability of ABTe$_2$ compounds to be good candidates for light energy conversion has been theoretically studied at the DFT level of calculation using the PBE0 exchange-correlation energy functional. The cell parameters are in agreement with the experimental and available theoretical results. The dielectric constant and exciton binding energy are investigated for the first time for these materials. The electronic and optical properties of ABTe$_2$ compounds have been also performed. The studied compounds have an indirect energy band gap, and the analysis of the total density of states shows that all bands gap energies are described by [B^{+3}-Te^{-2}] electronic transitions. Important fundamental properties such as band gap, effective mass, dielectric constant, and exciton binding energy have been calculated and present the efficiency of these compounds in light energy conversion. It can be concluded that among all the considered ternary compounds, the fundamental static properties for NaYTe$_2$, LiYTe$_2$ and RbYTe$_2$ are more attractive for applications of solar light energy conversion. Linear optical spectra of ABTe$_2$ were discussed and present an anisotropic character. When the atomic number of the alkali metal increases the peak width decreases and their position is shifted towards higher energy. Apart from the cell parameters and some electronic properties of the studied materials, no data on these materials was found in the literature for comparison, therefore further theoretical and experimental studies are suggested to exploit the real potential of these materials for practical applications.

References

[1] V. Kamat Prashant, Meeting the clean energy demand: nanostructure architectures for solar energy conversion, J. Phys. Chem. C 111 (2007) 2834–2860, https://doi.org/10.1021/jp066952u.

[2] T. Le Bahers, M. Rérat, P. Sautet, Semiconductors used in photovoltaic and photocatalytic devices:assessing fundamental properties from DFT, J. Phys. Chem. C 118 (2014) 5997–6008, https://doi.org/10.1021/jp409724c.

[3] Q. Xu, D. Yang, J. Lv, Y.-Y. Sun, L. Zhang, Perovskite solar absorbers: materials by design, Small Methods (2018) 1700316, https://doi.org/10.1002/smtd.201700316, 1700316.

[4] S.S. Abed Al- Abbas, M.K. Muhsin, H.R. Jappor, Tunable optical and electronic properties of gallium telluride monolayer for photovoltaic absorbers and ultraviolet detectors, Chem. Phys. Lett. 713 (2018) 46–51, https://doi.org/10.1016/J.CPLETT.2018.10.020.

[5] H.R. Jappor, M.M. Obeid, T.V. Vu, D.M. Hoat, H.D. Bui, N.N. Hieu, S.J. Edrees, Y. Mogulkoc, R. Khenata, Engineering the optical and electronic properties of Janus monolayer Ga$_2$SSe by biaxial strain, Superlattice Microstruct. 130 (2019) 545–553, https://doi.org/10.1016/J.SPMI.2019.05.031.

[6] H.D. Bui, H.R. Jappor, N.N. Hieu, Tunable optical and electronic properties of Janus monolayers Ga$_2$SSe, Ga$_2$STe, and Ga$_2$SeTe as promising candidates for ultraviolet photodetectors applications, Superlattice Microstruct. 125 (2019) 1–7, https://doi.org/10.1016/j.spmi.2018.10.020.

[7] M.M. Obeid, M.M. Shukur, S.J. Edrees, R. Khenata, M.A. Ghebouli, S.A. Khandy, A. Bouhemadou, H.R. Jappor, X. Wang, Electronic band structure, thermodynamics and optical characteristics of BeO$_{1-x}$A$_x$(A = S, Se, Te) alloys: insights from ab initio study, Chem. Phys. 526 (2019) 110414, https://doi.org/10.1016/J.CHEMPHYS.2019.110414.

[8] M.M. Obeid, H.R. Jappor, S.J. Edrees, M.M. Shukur, R. Khenata, Y. Mogulkoc, The electronic, half-metallic, and magnetic properties of Ca$_{1\text{-}x}$Cr$_x$S ternary alloys: insights from the first-principle calculations, J. Mol. Graph. Model. 89 (2019) 22–32, https://doi.org/10.1016/J.JMGM.2019.02.004.

[9] R.R. Lunt, T.P. Osedach, P.R. Brown, J.A. Rowehl, V. Bulović, Practical roadmap and limits to nanostructured photovoltaics, Adv. Mater. 23 (2011) 5712–5727, https://doi.org/10.1002/adma.201103404.

[10] J. Zhang, T. Ruf, R. Lauck, M. Cardona, Isotope effects on exciton energies in CdS, Phys. Rev. B. 57 (1998) 9716–9722, https://doi.org/10.1142/2508.

[11] T. Taguchi, J. Shirafuji, Y. Inuishi, Excitonic emission in cadmium telluride, Phys. Status Solidi 68 (1975) 727–738, https://doi.org/10.1002/pssb.2220680234.

[12] A. Teke, Ü. Özgür, S. Doğan, X. Gu, H. Morkoç, B. Nemeth, J. Nause, H.O. Everitt, Excitonic fine structure and recombination dynamics in single-crystalline ZnO, Phys. Rev. B. 70 (2004) 1–10, https://doi.org/10.1103/PhysRevB.70.195207.

[13] J. Pelant, Ivan, Valenta, Luminescence Spectroscopy of Semiconductors, Oxford University Press, 2012.

[14] Madelung Otfried, Semiconductors: Data Handbook, Springer Science & Business Media, 2012.

[15] H.R. Jappor, Band-structure calculations of GaAs within semiempirical large unit cell method, Eur. J. Sci. Res. 59 (2011) 264–275.

[16] S. Adachi, GaAs and Related Materials: Bulk Semiconducting and Superlattice Properties, World Scientific Publishing Co. Pte. Ltd, 1994, https://doi.org/10.1142/2508.

[17] I. Vurgaftman, J.R. Meyer, L.R. Ram-Mohan, Band parameters for III-V compound semiconductors and their alloys, J. Appl. Phys. 89 (2001) 5815–5875, https://doi.org/10.1063/1.1368156.

[18] M. Henini, Semiconductors: data handbook, Microelectron. J. 35 (2004) 685, https://doi.org/10.1016/j.mejo.2004.04.001.

[19] K. Stöwe, C. Napoli, S. Appel, Synthesen und Kristallstrukturen von neuen Alkalimetall-Selten-Erd- Telluriden der Zusammensetzungen KLnTe$_2$ (Ln = La, Pr, Nd, Gd), RbLnTe$_2$ (Ln = Ce, Nd) und CsLnTe$_2$ (Ln = Nd), Zeitschrift Fur Anorg. Und Allg. Chemie. 629 (2003) 1925–1928, https://doi.org/10.1002/zaac.200300167.

[20] J.M. Babo, T. Schleid, Two alkali-metal yttrium tellurides: single crystals of trigonal KYTe 2 and hexagonal RbYTe$_2$, Zeitschrift Fur Anorg. Und Allg. Chemie. 635 (2009) 1160–1162, https://doi.org/10.1002/zaac.200900029.

[21] J. Shi, T.F.T. Cerqueira, W. Cui, F. Nogueira, S. Botti, M.A.L. Marques, High-throughput search of ternary chalcogenides for p-type transparent electrodes, Sci. Rep. 7 (2017) 1–13, https://doi.org/10.1038/srep43179.

[22] V. Jarỳ, L. Havlák, J. Bárta, M. Buryi, E. Mihóková, M. Rejman, V. Laguta, M. Nikl, Optical, structural and paramagnetic properties of Eu-doped ternary sulfides ALnS$_2$ (A = Na, K, Rb; Ln = La, Gd, Lu, Y), Materials (Basel) 8 (2015) 6978–6998, https://doi.org/10.3390/ma8105348.

[23] V. Jarý, L. Havlák, J. Bárta, E. Mihóková, P. Průša, M. Nikl, Optical properties of Eu^{2} $^{+}$-doped KLuS^{2} phosphor, Chem. Phys. Lett. 574 (2013) 61–65. https://doi.org/10.1016/j.cplett.2013.05.001.

[24] V. Jarý, L. Havlák, J. Bárta, E. Mihóková, M. Nikl, Luminescence and structural properties of RbGdS$_2$ compounds doped by rare earth elements, Opt. Mater. 35 (2013) 1226–1229, https://doi.org/10.1016/j.optmat.2013.01.028.

[25] L. Havlák, V. Jarý, M. Nikl, P. Boháček, J. Bárta, Preparation, luminescence and structural properties of RE-doped RbLaS$_2$ compounds, Acta Mater. 59 (2011) 6219–6227, https://doi.org/10.1016/j.actamat.2011.06.019.

[26] L. Havlák, V. Jarý, M. Rejman, E. Mihóková, J. Bárta, M. Nikl, Luminescence characteristics of doubly doped KLuS$_2$:Eu, RE (RE = Pr, Sm, Ce), Opt. Mater. 41 (2015) 94–97, https://doi.org/10.1016/j.optmat.2014.08.002.

[27] V. Jarý, L. Havlák, J. Bárta, E. Mihoková, M. Buryi, M. Nikl, ALnS$_2$:RE (A=K, Rb; Ln=La, Gd, Lu, Y): new optical materials family, J. Lumin. 170 (2016) 718–735, https://doi.org/10.1016/j.jlumin.2015.08.080.

[28] C.L. Teske, W. Bensch, A. Perlov, H. Ebert, Preparation, crystal structure, physical properties, and electronic band structure of $TlTaS_3$, Z. Anorg. Allg. Chem. 628 (2002) 1511–1516, https://doi.org/10.1002/zaac.200700440.

[29] I. Khan, I. Ahmad, D. Zhang, H.A. Rahnamaye Aliabad, S. Jalali Asadabadi, Electronic and optical properties of mixed Be-chalcogenides, J. Phys. Chem. Solids 74 (2013) 181–188, https://doi.org/10.1016/j.jpcs.2012.08.012.

[30] M. Safari, Z. Izadi, J. Jalilian, I. Ahmad, S. Jalali-Asadabadi, Metal mono-chalcogenides ZnX and CdX (X = S, Se and Te) monolayers: chemical bond and optical interband transitions by first principles calculations, Phys. Lett. Sect. A Gen. At. Solid State Phys. 381 (2017) 663–670, https://doi.org/10.1016/j.physleta.2016.11.040.

[31] L. Tairi, S. Touam, A. Boumaza, M. Boukhtouta, H. Meradji, S. Ghemid, S. Bin Omran, F.E.H. Hassan, R. Khenata, Phase stability and electronic behavior of MgS, MgSe and MgTe compounds, Phase Transitions 90 (2017) 929–941, https://doi.org/10.1080/01411594.2017.1302085.

[32] W. Kohn, L.J. Sham, Self-consistent equations including exchange and correlation effects, Phys. Rev. 140 (1965), https://doi.org/10.1103/PhysRev.140.A1133.

[33] R. Dovesi, A. Erba, R. Orlando, C.M. Zicovich-Wilson, B. Civalleri, L. Maschio, M. Rérat, S. Casassa, J. Baima, S. Salustro, B. Kirtman, Quantum-mechanical condensed matter simulations with CRYSTAL, Wiley Interdiscip. Rev. Comput. Mol. Sci. 8 (2018) 1–36, https://doi.org/10.1002/wcms.1360.

[34] J.P. Perdew, K. Burke, M. Ernzerhof, Generalized gradient approximation made simple, Phys. Rev. Lett. 77 (1996) 3865–3868, https://doi.org/10.1103/PhysRevLett.77.3865.

[35] C. Adamo, V. Barone, Toward reliable density functional methods without adjustable parameters: the PBE0 model, J. Chem. Phys. 110 (1999) 6158–6170, https://doi.org/10.1063/1.478522.

[36] J. Heyd, G.E. Scuseria, M. Ernzerhof, Erratum: hybrid functionals based on a screened Coulomb potential (journal of chemical physics (2003) 118 (8207)), J. Chem. Phys. 124 (2006), https://doi.org/10.1063/1.2204597.

[37] J. Heyd, G.E. Scuseria, M. Ernzerhof, Hybrid functionals based on a screened Coulomb potential, J. Chem. Phys. 118 (2003) 8207–8215, https://doi.org/10.1063/1.1564060.

[38] R. Dovesi, C. Ermondi, E. Ferrero, C. Pisani, C. Roetti, Hartree-Fock study of lithium hydride with the use of a polarizable basis set, Phys. Rev. B. 29 (1984) 3591–3600, https://doi.org/10.1103/PhysRevB.29.3591.

[39] R. Dovesi, C. Roetti, C. Freyria-Fava, M. Prencipe, V.R. Saunders, On the elastic properties of lithium, sodium and potassium oxide. An ab initio study, Chem. Phys. 156 (1991) 11–19, https://doi.org/10.1016/0301-0104(91)87032-Q.

[40] CRYSTAL code website, http://www.crystal.unito.it/basis-sets.php.

[41] T. Bredow, K. Jug, R.A. Evarestov, Electronic and magnetic structure of $ScMnO_3$, Phys. Status Solidi 243 (2006) R10–R12, https://doi.org/10.1002/pssb.200541403.

[42] J. Heyd, J.E. Peralta, G.E. Scuseria, R.L. Martin, Energy band gaps and lattice parameters evaluated with the Heyd-Scuseria-Ernzerhof screened hybrid functional, J. Chem. Phys. 123 (2005), https://doi.org/10.1063/1.2085170.

[43] H.J. Monkhorst, J.D. Pack, Special points for Brillouin-zone integrations, Phys. Rev. B. 13 (1976) 5188–5192.

[44] T.H. Fischer, J. Almlof, General methods for geometry and wave function optimization, J. Phys. Chem. 96 (1992) 9768–9774, https://doi.org/10.1021/j100203a036.

[45] A.M. Ferrari, R. Orlando, M. Rérat, Ab initio calculation of the ultraviolet-visible (UV-vis) absorption spectrum, electron-loss function, and reflectivity of solids, J. Chem. Theory Comput. 11 (2015) 3245–3258, https://doi.org/10.1021/acs.jctc.5b00199.

[46] B. Deng, D.E. Ellis, J.A. Ibers, New layered rubidium rare-earth selenides: syntheses, structures, physical properties, and electronic structures for $RbLnSe_2$, Inorg. Chem. 41 (2002) 5716–5720, https://doi.org/10.1021/ic020324j.

[47] L.J. Butts, N. Strickland, B.R. Martin, Synthesis of layered sodium lanthanum selenide through ion exchange reactions, Mater. Res. Bull. 44 (2009) 854–859, https://doi.org/10.1016/j.materresbull.2008.09.012.

[48] R. Ballestracci, E.F. Bertaut, Étude cristallographique de sulfures de terres rares et de sodium, Bull. LA Soc. Fr. Mineral. Cristallogr. 87 (1964) 512–517.

[49] D. Ma, W. Ju, Y. Tang, Y. Chen, First-principles study of the small molecule adsorption on the InSe monolayer, Appl. Surf. Sci. 426 (2017) 244–252, https://doi.org/10.1016/J.APSUSC.2017.07.198.

[50] M.M. Obeid, H.R. Jappor, K. Al-Marzoki, D.M. Hoat, T.V. Vu, S.J. Edrees, Z.M. Yaseen, M.M. Shukur, Electronic and magnetic properties of single-layer boron phosphide associated with materials processing defects, Comput. Mater. Sci. 170 (2019) 109201, https://doi.org/10.1016/J.COMMATSCI.2019.109201.

[51] M.G. Ju, J. Dai, L. Ma, X.C. Zeng, Perovskite chalcogenides with optimal bandgap and desired optical absorption for photovoltaic devices, Adv. Energy Mater. 7 (2017) 2–8, https://doi.org/10.1002/aenm.201700216.

[52] G.J.B. Hurst, M. Dupuis, E. Clementi, Ab initio analytic polarizability, first and second hyperpolarizabilities of large conjugated organic molecules: applications to polyenes C4H6to C22H24, J. Chem. Phys. 89 (1988) 385–395, https://doi.org/10.1063/1.455480.

[53] A.V. Rodina, M. Dietrich, A. Göldner, L. Eckey, A. Hoffmann, A.L. Efros, M. Rosen, B.K. Meyer, Free excitons in wurtzite GaN, Phys. Rev. B. 64 (2001) 115204, https://doi.org/10.1103/PhysRevB.64.115204.

[54] S. Marques, A.L. Miguel, Julien Vidal, Micael JT. Oliveira, Lucia Reining, Botti, Density-based mixing parameter for hybrid functionals, Phys. Rev. B. 83 (2011), 035119.

[55] J.C. Conesa, Band structures and nitrogen doping effects in zinc titanate photocatalysts, Catal. Today 208 (2013) 11–18, https://doi.org/10.1016/j.cattod.2012.08.039.

[56] H. He, R. Orlando, M.A. Blanco, R. Pandey, E. Amzallag, I. Baraille, M. Rérat, First-principles study of the structural, electronic, and optical properties of Ga_2O_3 in its monoclinic and hexagonal phases, Phys. Rev. B. 74 (2006) 195123.

[57] V. Fiorentini, Dielectric scaling of the self-energy scissor operator in semiconductors and insulators, Phys. Rev. 8 (51) (1995) 196–198.

[58] V.L. Shaposhnikov, A.V. Krivosheeva, V.E. Borisenko, Ab initio modeling of the structural, electronic, and optical properties of ABC2 semiconductors, Phys. Rev. B. 85 (2012) 205201, https://doi.org/10.1103/PhysRevB.85.205201.

[59] A.H. Reshak, K. Nouneh, I.V. Kityk, J. Bila, S. Auluck, H. Kamarudin, Z. Sekkat, Structural , electronic and optical properties in earth- abundant photovoltaic absorber of Cu_2ZnSnS_4 and $Cu_2ZnSnSe_4$ from DFT calculations, Int. J. Electrochem. Sci. 9 (2014) 955–974.

[60] O.L. Muskens, J.G. Rivas, R.E. Algra, E.P.A.M. Bakkers, A. Lagendijk, Design of light scattering in nanowire materials for photovoltaic applications, Nano Lett. 8 (2008) 2638–2642, https://doi.org/10.1021/nl0808076.

[61] C. Martinet, V. Paillard, A. Gagnaire, J. Joseph, Deposition of SiO_2 and TiO_2 thin films by plasma enhanced chemical vapor deposition for antireflection coating, J. Non-Cryst. Solids 216 (1997) 77–82, https://doi.org/10.1016/S0022-3093(97)00175-0.

[62] J. Aiken Daniel, Antireflection coating design for series interconnected multi-junction solar cells, Prog. Photovoltaics. 8 (2000) 563–570, https://doi.org/10.1002/1099-159X(200011/12)8:6<563::AID-PIP327>3.0.CO;2-8.

[63] J. Zhao, M.A. Green, Optimized antireflection Coatings for high-efficiency silicon solar cells, IEEE Trans. Electron Devices 38 (1991), https://doi.org/10.1109/16.119035.